Bulgarian Chemical Communications, Volume 57, Issue 4 (pp. 319-330) 2025 DOI: 10.34049/bcc.57.4.5657

Modeling of blood flow in a stenotic artery using nanoparticles

Priyanshu, M. M. Mandal*

University School of Chemical Technology, Guru Gobind Singh Indraprastha University, New Delhi – 110078, India

Received: July 15, 2024; Revised: September 29, 2025

In recent years, investigations have been conducted to understand the influence of nanoparticles on blood flow *via* stenosed arteries. The purpose of the present study was to investigate the hydrodynamics and heat transfer of blood flow carrying metallic nanoparticles through a stenotic artery. A computational fluid dynamics study was conducted using COMSOL Multiphysics software to solve the governing equations with appropriate boundary conditions and thermophysical models. Different viscous models were applied and compared to model the viscosity of blood flow. The blood flow velocity, shear stress, and temperature contours of the stenotic artery were investigated for different dimensions. The magnetic field's impact on blood flowing through stenosis is reported here. The findings suggest that the effect of the viscous model for blood could be significant for arteries with smaller sizes. Applying a magnetic field to the stenosis resulted in reduced fluid velocity and higher shear stress near the wall in arteries with smaller dimensions. This model can help screen different anti-angiogenic drugs used in the treatment of stenotic arteries. The present study can further benefit the design of a technology for drug delivery in stenotic arteries using drugs with magnetic properties.

Keywords: Computational fluid dynamics, stenotic artery, nanoparticle, magnetic field, viscosity

INTRODUCTION

Arterial stenosis, also known as blood artery narrowing, is a serious medical condition that can result in cardiovascular illnesses. Arterial diseases, such as arterial stenosis, obstruct blood flow and impact blood pressure, contributing to cardiovascular complications. This progressive disease affects a significant number of individuals, particularly those aged 75 and above. In India, even those marginally older than 45 years of age have a significant prevalence of cardiovascular illnesses [1]. Arterial stenosis, characterized by narrowing of arteries, poses a serious threat and is a leading cause of mortality in both underdeveloped and developed countries. Its causes, symptoms, and complications are well-documented. Lipid accumulation in the vascular system might contribute to the progression of stenosis in blood vessels. Lesions in the arteries can result from the formation of stenosis, which narrows the blood vessels. The circulatory system relies on blood vessels to transport oxygen and nutrients, and remove waste products, making blood flow dynamics crucial in the development and progression of cardiovascular diseases. Significant changes to the flow characteristics within the arteries can be caused by stenosis and aneurysms. One of the severe consequences of arterial stenosis is increased resistance and reduced blood flow through the affected artery.

For the development of efficient therapeutic approaches, it is essential to comprehend the flow properties and heat transfer processes within stenotic arteries. Various researchers have focused on studying arterial diseases using different methods. Recent studies have explored the incorporation of nanomaterials in base fluids. Several theoretical studies have also been carried out to comprehend how the concentration of nanoparticles affects blood flow through stenosed arteries [2–6]. A particular kind of fluid called a nanofluid has nanoparticles that have been carefully engineered (size varying from 1 to 100 nm) and dispersed in a fluid medium. Nanomaterials such as carbon in different forms, metals, and nanostructures are often utilized in nanofluids. Researchers have used nanoparticles for enhancing heat transfer, studying blood flow through stenoses, and analyzing two or three-dimensional flow models [2–5]. It has been demonstrated that the use of nanofluids, which are fluids containing metallic nanoparticles, can improve heat transfer efficiency in a variety of applications. Various nanoparticles have several applications in diagnostics and treatment of cardiovascular diseases, offering improved treatment strategies and targeted delivery into arteries based on their physical properties, such as shape, surface, and size modifications. Nanoparticles like silver and gold are particularly significant in nanomedicine, serving as drug carriers, photovoltaic agents, and contrast

* To whom all correspondence should be sent:
E-mail: *monishamridha1@ipu.ac.in*

agents [2, 3, 7]. Their unique properties make them attractive for biomedical diagnosis and treatment. Applications for gold nanoparticles in biomedicine are numerous and include targeted drug delivery, immunological modulation, diagnostics, therapies, gene delivery, cancer treatment, and prosthetics. Silver nanoparticles are also gaining importance in the fields of visual imaging, medicinal sciences, catalysis, anti-angiogenic drugs, etc. [7]. Given their unique physicochemical characteristics, simple synthesis and characterization, variable shape and size, and biocompatibility, biologically produced silver nanoparticles are one of the most attractive choices in biomedical research.

Magnetic field has been shown to have a significant impact on the biological fluids present in all living organisms [9, 10]. Owing to haemoglobin presence, the blood is magnetically responsive. The paramagnetic properties of blood are due to the presence of Fe^{++} chains in deoxygenated haemoglobin [11]. When blood is exposed to an external magnetic field, it experiences both Lorentz and magnetization forces. Blood viscosity can be impacted by magnetic fields, particularly at higher levels [12]. Due to the increased apparent viscosity of blood caused by the magnetic field, it has been observed that the blood flow rate has decreased [13].

Studies of partially blocked arteries have shown that a magnetic field does not always decrease blood velocity; the effect varies depending on the direction of the applied magnetic field, with some orientations generating acceleration and others slowing down [14–16]. According to a study that developed a mathematical model treating blood as a Newtonian fluid, the dimensionless velocity magnitude is significantly reduced in a stenotic channel when a magnetic field is applied perpendicular to the direction of flow. Several researchers have investigated the combined effect of nanofluid flow under a magnetic field in arteries [6, 8, 9]. Elelamy *et al.* investigated the temperature distribution, slip effects, and blood flow with nanofluids in a heart valve. They observed that there can be a reduction in vascular resistance when the heart valve prosthesis induces a magnetic field. Vascular resistance values enhance the concentration of antibiotics and other compounds that can infiltrate bacteria. It has been found that as the magnetic field intensity increases, the temperature rises, and the velocity of the nanofluid decreases [17]. The strong, broad-spectrum antibacterial qualities of silver nanoparticles are enhanced by their large surface area due to particle size and capacity to release silver ions, making them useful against harmful bacteria, fungi, and viruses. They are also helpful in wound healing, drug delivery, tissue engineering, and as parts of medical devices and diagnostic instruments, owing to their anti-inflammatory, anti-cancer, and anti-angiogenic properties [18]. Silver nanoparticles are utilized in stenosis applications, including airway stents and endodontic treatments. They prevent infections and inflammation that lead to stenosis by releasing silver ions, which harm internal biological components, including proteins and DNA, and break down bacterial cell walls. Silver nanoparticles' anti-hyperplastic qualities also lessen the development of granulation tissue, which can lead to stenosis. Further, when dispersed to create nanofluids, silver's high thermal conductivity (429 W/m·K at ambient temperature) greatly improves the fluids' thermal characteristics and facilitates heat transfer, thus controlling the temperature of the blood flow. Hence, silver nanoparticles were considered for the present study. Since silver is a non-ferromagnetic substance, it lacks the inherent magnetic properties necessary to be drawn to a magnet. Silver nanoparticles in their original state do not respond to magnetic fields. However, by functionalizing with superparamagnetic elements like iron oxides, which create a transient magnetic response without permanently magnetizing the silver, these nanoparticles can be made responsive to magnetic fields [19].

The application of nanocomposites in treating vascular disorders is limited, and the use of silver nanoparticles in treating arterial diseases is still in the developmental stage. Therefore, the goal of the current investigation was to investigate the hydrodynamics of silver nanoparticles in blood flowing through a carotid stenosis artery. In this study, a mathematical model was developed to analyze the characteristics of blood flow with silver nanoparticles when artery stenosis is present. The simulation considered a 2D artery with a cosine-shaped stenosis, and the dimensions, as well as the initial conditions, were defined. The effect of different dimensions, magnetic field, and viscous models on the hydrodynamics of the nanofluid was investigated. Velocity distributions, shear stress contours, magnetic field, and temperature distributions of the nanofluid were obtained and reported here.

MATERIALS AND METHODS

The COMSOL Multiphysics software was used to numerically solve the Navier-Stokes equations to account for continuity, energy, and momentum conservation of the flow of blood with nanoparticles. Based on existing literature data, the shape of the stenotic artery was created, and the suitable

boundary conditions were applied [7]. For validation of the model with literature data, blood was assumed to flow through a stenosed artery as an incompressible Newtonian fluid. The equations for the fluid flow, heat convection, and conduction phenomena in conjunction with the suitable boundary conditions were computed. The continuity equation is:

$$\frac{1}{\mathrm{r}}\frac{\partial}{\partial \mathrm{r}}(\mathrm{ru})+\frac{\partial}{\partial \mathrm{z}}(\mathrm{w})=0 \quad (1)$$

$$\rho \nabla . u = 0 \quad (2)$$

where w and u correspond to the nanofluid's velocities in the z and r directions, respectively. In the present study, the Eulerian-Eulerian multiphase modeling approach was used, which treats the phases as interpenetrating continua with a no-slip condition assumed between them. In the Mixture model for nanofluid flow, nanoparticles were assumed to have the same velocity as the base fluid.

The governing momentum equation was computed as:

$$\rho_{(u_t+uu_r+wu_z)} = -P_r + \partial_z(w_r - u_z)\mu \quad (3)$$

$$\rho_{(w_t+uw_r+ww_z)} = -P_r - \left(\partial_r + \frac{1}{r}\right)(w_r - u_z)\mu \quad (4)$$

The equations can be written as:

$$\rho(u.\nabla u) = \nabla.[-PI + K] + F \quad (5)$$

$$K = \mu(\nabla u + (\nabla u)^T) \quad (6)$$

where μ and ρ represent the nanofluid's viscosity and density, respectively, P is the pressure, and I is the identity tensor.

The equation to calculate the wall shear stress (WSS) is given as [20]:

$$WSS = \mu \times \frac{\delta u}{\delta x}$$

The governing heat transfer equation was computed as:

$$\left(\rho C_p\right)\left(\frac{\partial}{\partial t} + u\frac{\partial}{\partial r} + w\frac{\partial}{\partial z}\right)T = k\left(\frac{\partial^2}{\partial r^2} + \frac{\partial}{r\partial r} + \frac{\partial^2}{\partial z^2}\right)T \quad (7)$$

$$d_z\rho C_p\frac{\partial T}{\partial t} + d_z\rho C_p u.\nabla T + \nabla.q = d_z Q + q_o + d_z Q_p + d_z Q_{vd} \quad (8)$$

where $q = -d_z k\nabla T$; $q_0 = \frac{q}{A_s\Delta T}$; $Q_{vd} = \tau.\nabla u$; $Q_p = \alpha_p T\left(\frac{\partial P}{\partial t} + u.\nabla P\right)$; $\alpha_P = -\frac{1}{\rho}\frac{\partial P}{\partial t}$; $\tau = -PI + K$; d_z is the thickness of the fluid; Q is the heat source; Q_{vd} is the viscous dissipated heat source; ∇T shows the temperature gradient; C_p is the specific heat; and k is the thermal conductivity of the nanofluid. The initial values considered are:

$$T=T_o \text{ and } P=0 \quad (9)$$

The thermophysical properties of the nanofluids are defined as follows [21, 22]:

$$\left.\begin{aligned} \rho &= \rho_f\left[(1-\phi) + \phi\left(\frac{\rho_s}{\rho_f}\right)\right] \\ \mu &= \frac{\mu_f}{(1-\phi)^{2.5}} \\ \left(\rho C_p\right) &= \left(\rho \mathrm{C_p}\right)_f\left[1 - \phi + \phi\frac{(\rho C_p)_s}{(\rho C_p)_f}\right] \\ \frac{k}{k_f} &= \frac{k_s+(s-1)k_f-(s-1)\emptyset(k_f-k_s)}{k_s+(s-1)k_f+\emptyset(k_f-k_s)} \end{aligned}\right\} \quad (10)$$

where ϕ is the volume fraction of the dispersed phase, silver nanoparticles; μ_f is the viscosity of the fluid (blood); ρ_f is the continuous phase (blood) density; ρ_s is the discrete phase (silver nanoparticles) density; k_f is the thermal conductivity of the fluid (blood); k_s is the thermal conductivity of the solid nanoparticles; $\left(\rho C_p\right)_s$ is the heat capacity of the solid nanoparticles; $\left(\rho C_p\right)_f$ is the heat capacity of the fluid.

Magnetic field

To determine the effect of the magnetic field, an AC/DC module in COMSOL Multiphysics was used. The formulae for the Ampere-Maxwell equation that were used to calculate the static magnetic field are as follows [23]:

$$\nabla \times \bar{H} = \bar{J} \quad (11)$$

The magnetic flux density using Gauss's law is:

$$\nabla . B = 0 \quad (12)$$

Here, H is the strength of the magnetic field; B represents the magnetic flux density.

The relationship between B and H, provided by the following formulas, can be used to characterize the magnetic flux density for stenotic domains:

$$\bar{B} = \mu_0\left(\bar{H} + \overline{M_b}(H)\right) \quad (13)$$

where μ_0 is the magnetic permeability of blood; the blood stream's magnetization vector (A/m) is defined as $M_b(H)$, and it depends on the magnetic field, H.

The body force acting on a fluid flow was calculated using Maxwell's electromagnetic equation. The Magnetic Fields, No Currents, Boundary Elements interface in COMSOL Multiphysics was employed to compute magnetostatic fields from permanent magnets and other current-free magnetic sources. The physics interface solves Gauss' Law for the magnetic field using the scalar magnetic potential as the dependent variable. Stress tensors under the influence of magnetic fields were computed using Maxwell's

equations of electromagnetic force [24]. Volume forces acting on a body in electromagnetic fields were included to estimate electromagnetic forces. τ_{xx} and τ_{yy} are the typical stress tensors operating in the x and y axes, respectively. The shear stress tensors in the x and y directions were taken to be $\tau_{xy} = \tau_{yx}$ for a fixed-volume system. The divergence of the stress tensors yields the volume force throughout the body. For blood flow in the arterial channel, eq. 18 calculates the magnetic forces F_x and F_y in the x and y directions, respectively. These forces show up in the Navier-Stokes equations as volume forces F and are coupled with Gauss' Law.

$$T_{xx} = \frac{1}{2\mu_0\mu_r}\left(B_x^2 - B_y^2\right) \quad (14)$$

$$T_{yy} = \frac{1}{2\mu_0\mu_r}\left(B_y^2 - B_x^2\right) \quad (15)$$

$$T_{xy} = T_{yx} = \frac{1}{\mu_0\mu_r}\left(B_x B_y\right) \quad (16)$$

The stress tensor is written as:

$$T = \begin{bmatrix} T_{xx} & T_{xy} \\ T_{yx} & T_{yy} \end{bmatrix} \quad (17)$$

The volume force was calculated using the equation:

$$F = \nabla . T \quad (18)$$

Boundary conditions

The boundary conditions were set at the inlet, outlet, and wall in the laminar flow module of COMSOL Multiphysics software. The velocity and area of the inflow passage were utilized to control the blood volume. The boundary condition for the inlet was as follows [7]:

$u(r, z, t) = - u_o n$

The location of the outlet was where the blood left the artery and was located across from the entrance. A solution of the governing equations was obtained at the outlet. The following was the outlet's boundary condition:

$\tau n = -p n,$

where $p = p_o$, the absolute pressure was $p_o=0$ and $\boldsymbol{n} = (\boldsymbol{n}_r, \boldsymbol{n}_z)$ was the normal outflow velocity.

The no-slip condition was set at the wall of the artery, which meant that the bulk blood's velocity was zero.

$u=0, w=0$

Thermal insulation was used by the following equation using the heat transfer module in the COMSOL software at the inlet and outlet boundaries:

$n.q =0$

It has been reported that treating cardiovascular disorders requires an understanding of heat transport in stenotic arteries since it aids in determining the degree of stenosis, forecasting risks such as ischemic stroke, and directing therapies like targeted drug delivery or heat-based therapies [25]. Therefore, in the present study, different temperatures were considered on the top wall and lower wall as an initial condition to understand the effect of the heat transfer mechanism on the blood flow. This helped to understand the changes in temperature around the specific location within an artery, especially around the plaque. The initial temperature of blood was considered as 293.15 K. Temperature was 297.15 K at the top boundary wall, whereas it was considered 300.15 K at the bottom boundary wall. In computational fluid dynamics (CFD), the quality of the computational mesh is essential. The mesh quality affects both the convergence rate and the precision of the solution. The physical controlled mesh function in COMSOL creates the mesh automatically. When compared to a standard-size mesh, a finer element size mesh typically yields higher performance and more precise outcomes. To find the best mesh needed for the computation, a grid independence test was carried out. The finer mesh option was used in this study and is shown in Fig. 1. The mesh is more refined in the stenosed area and near the wall.

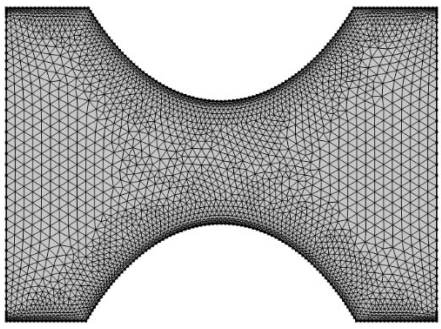

Fig. 1. Mesh of stenotic artery geometry

Consideration was given to the nanofluid's physical and chemical composition, including the characteristics of blood and silver nanoparticles. The computer model takes into account the thermophysical characteristics, including density, thermal conductivity, and specific heat capacity. The different viscous models were used in this study to explore the non-Newtonian effect of blood flow in arteries with different dimensions. The parameters used for modeling the blood dynamic viscosity μ as a function of the strain rate γ in the models employed are as follows [26, 27]:

In the Newtonian model, μ = 0.0035 Pa·s was considered. In the Power law model, $\mu = \mu_0 \gamma^{n-1}$ where μ_0 = 0.035 Pa·s and n = 0.6 was used for computation. In the Carreau model, $\mu = \mu_\infty + (\mu_0 - \mu_\infty)[1 + (\lambda\gamma)^2]^{\frac{n-2}{2}}$ where the viscosity at zero shear rate is μ_0 = 0.056 Pa.s, and at high shear rate μ_∞ equals the value for the Newtonian model (i.e., 0.0035 Pa.s) [27]. Additionally, n = 0.3568 and λ = 3.313 s. Using the above methodology, computations were carried out. The following section presents the results obtained from the computations and their analysis.

RESULTS AND DISCUSSION

The artery was first considered with dimensions of 1.1 m long and 0.8 m wide to validate the present model with known data in the literature [7]. The process conditions and dimensions of the artery as reported by Hussain *et al.* (2022) [7] were considered in the present study. Figs. 2 and 3 show the velocity contours and pressure contours computed from the present model, as well as the results of Hussain *et al*. (2022) [7] for the same process conditions and artery dimensions. Fig. 2(a) shows the blood flow velocity from the present computation, whereas Fig. 2(b) shows the blood velocity reported in the literature. The figure sheds light on the characteristics of blood flow behavior in the stenotic artery region. Maximum blood flow was seen at the stenotic artery, which is indicated by the color red. The blue color near the wall of the artery shows the minimum velocity because of the no-slip condition. The figure shows that the velocity computed from the current model was in good agreement with the literature. Fig. 3(a) shows the pressure variations due to the flow of blood through the stenotic artery obtained from the present computations. This was compared with the result cited in literature and shown here in Fig. 3(b). The pressure contours were found to be minimal at the center of the stenotic artery following the continuity equation. Two circular zones were found near the location of artery expansion. This was due to the reason that when the stenotic artery expands, the blood separates from the artery wall with high velocity, just as a jet. The space between the blood jet and the artery wall could be filled with blood in a vortex motion. This leads to a change in pressure after the blood passes through the contracted zone. The pressure contour from the present computation agreed well with the literature. This showed that the model worked well. Researchers have considered blood as a Newtonian fluid for computations [28].

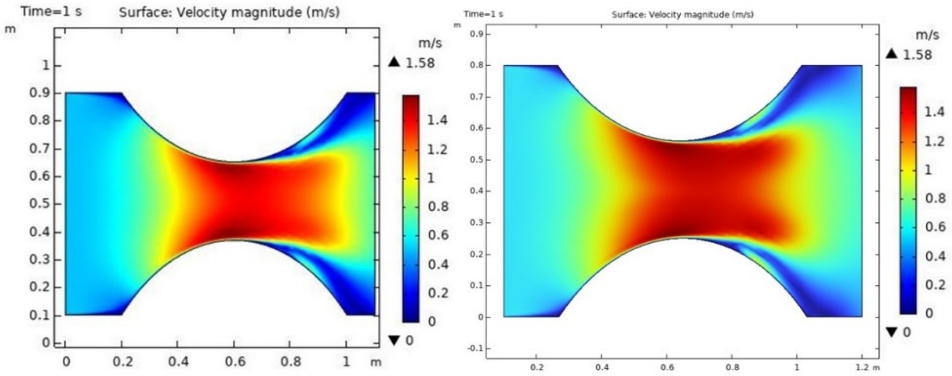

(a) (b)

Fig. 2. Velocity in a stenotic artery from (a) present model, (b) ref. [7]

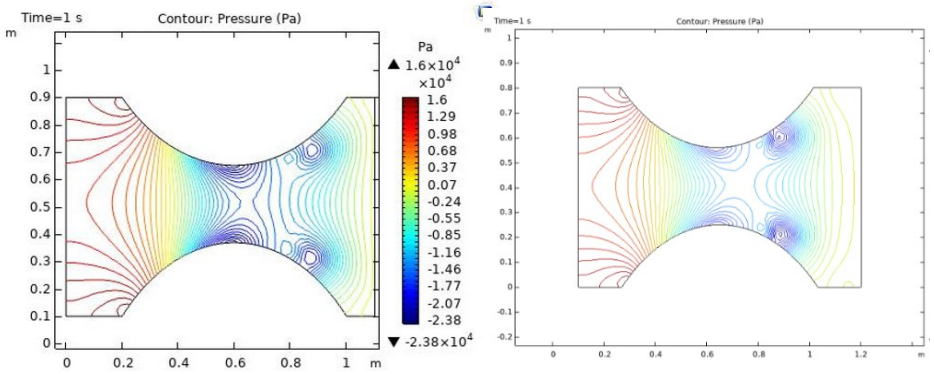

(a) (b)

Fig. 3. Pressure contours in a stenotic artery using (a) the present model, (b) ref. [7].

However, this viscous model may not be true for cases of aneurysmal arteries and overestimates the intracranial aneurysm domes' wall shear stress, displaying local flow recirculation and low shear rates [28, 29]. Therefore, different non-Newtonian viscous models, which included the Carreau model and the Power law model, were considered to check their effect in the present study. Fig. 4 shows the velocity of blood flow with nanoparticles using the different models for a 0.8 m wide artery at different times. The figure shows that the maximum velocity was at the stenosis region at time 0.2 min. In the Newtonian fluid, small peaks in maximum velocity in the core red region could be found after the blood flows through the stenosis region in the downstream.

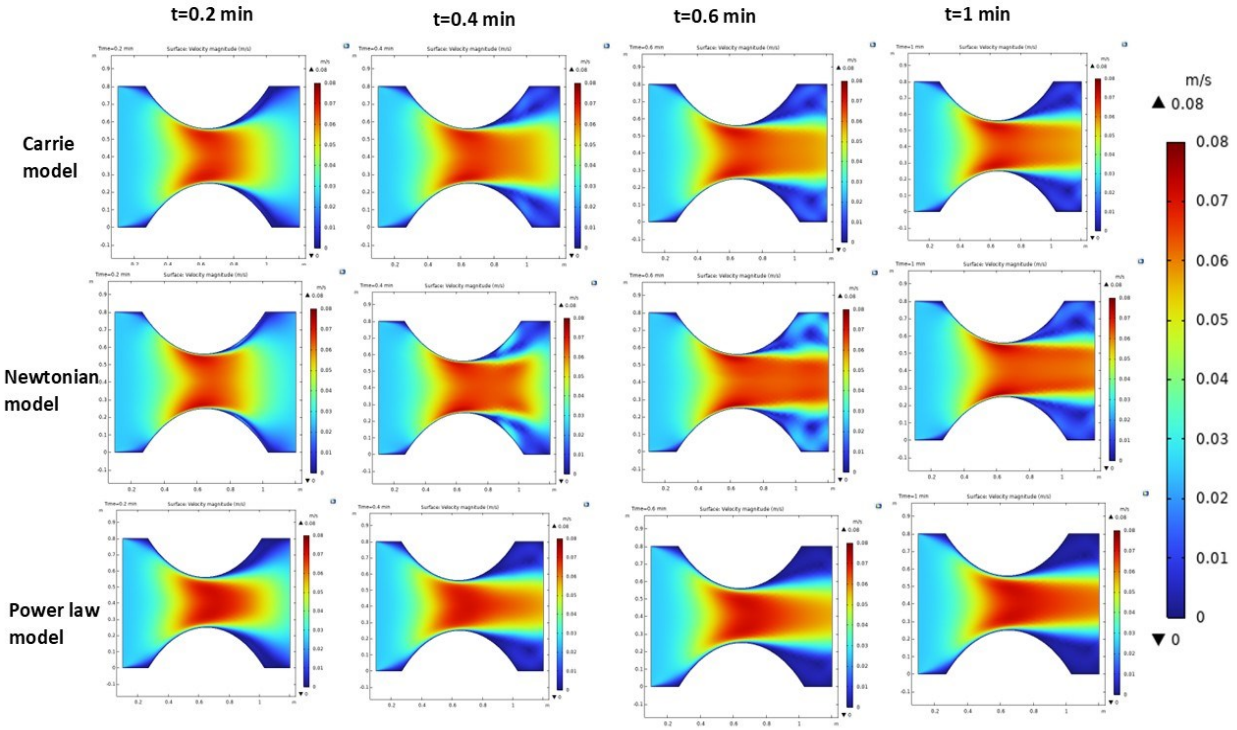

Fig. 4. Velocity in a stenotic artery using different models for d=0.8 m, v=0.025 m/s

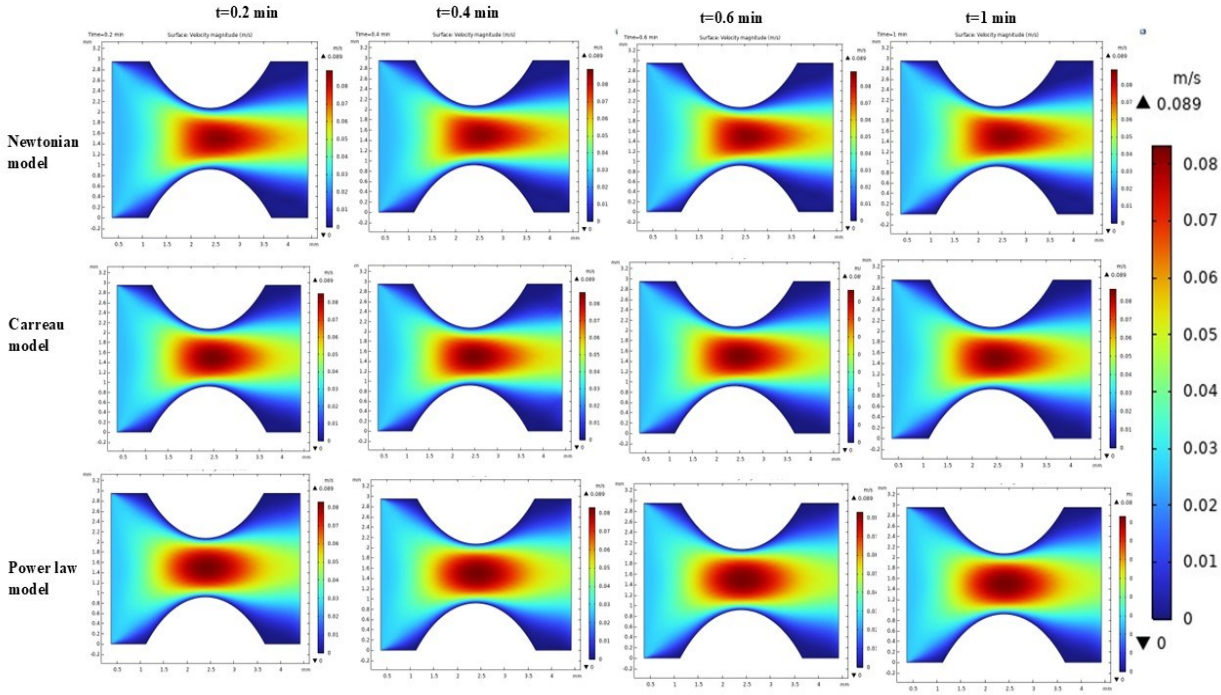

Fig. 5. Velocity in a stenotic artery for d=0.00295 m, v=0.025 m/s

In the case of the Carreau model and the Power law model, no such peaks were found. The velocity was found to be flatter and parabolic at times t=0.2 min and 0.4 min. The maximum velocity stretched out in the downstream of the stenosis with an increase in time. At the downstream region after the stenosis, velocity near the wall was nearly zero in the Power law model at 0.6 and 1 min. Due to the Carreau model's limitation on the viscosity's reduction with increasing strain, the change in velocity is similar to that of a Newtonian fluid. However, for the Power Law model, this is not the case. Fig. 4 clearly shows the developing velocity distribution of blood at different times till 1 min. After 1 min, there was no significant change in velocity. This showed that the blood flow was at steady state at 1 min.

Literature shows that the width of the left coronary artery could be smaller than 8 mm [30, 31]. This is due to branching patterns such as bifurcation and trifurcation of arteries. Therefore, the present model was used to study the artery with a width of 0.00295 m, as shown in Fig. 5. Research using a Newtonian model and presuming that shear rates are consistently higher than 100 s^{-1} can be considered as oversimplification of the blood flow since the instantaneous shear rate in numerous arteries fluctuates from 0 to 1000 s^{-1} over the course of one cardiac cycle [29, 32]. Therefore, different viscous models, such as the Power law model and Carrie model, were applied for blood flow with nanofluids to check the effect on blood flow velocity. It is observed from the figure that the velocity was highest at the center of the stenosis in accordance with the continuity equation and higher than the velocity (depicted in dark red color) in the artery with 0.8 m. The viscous sublayer (in blue color) near the wall was more than that in the artery with d=0.8 m. The maximum velocity in the Power law model was less stretched out in the downstream of the stenotic region as compared to the Newtonian model. This could be due to the characteristic of the Power law model to shear thin because of its viscosity reducing under strain. The Carreau fluid exhibited Power law behavior at high shear rates and Newtonian behavior at low shear rates. It was further observed that there was no change in velocity distribution after 0.2 min for blood flow in an artery with a smaller dimension, d=0.00295 m, as shown in Fig. 5. This showed that the steady state was already achieved. It took less time to get to a steady state in an artery with smaller dimensions as compared to a larger artery with d=0.8 m.

Effect of the magnetic field

Using nanoparticles in combination with an applied magnetic field has generated a lot of interest as a way to minimize the effects on surrounding tissue while controlling the release and accumulation of drugs in target tissues, because biological tissues respond very little to magnetic fields. When there is a magnetic field present, the magnetophoretic force attracts the particles in the vicinity of the illness site and has sufficient strength to push them into the tissue. To comprehend the contours that resulted from the magnetic field, computations were conducted for the stenosed vessel, as well as the normal vessel having the same boundary conditions. In this study, a magnetic field of 1 T was applied to the stenotic wall. The magnetic field that was applied to the blood flow was perpendicular to the artery axis and permeated the entire artery [33]. The distribution and magnitude of magnetic field strength with and without stenosis of the artery were studied, as illustrated in Fig. 6.

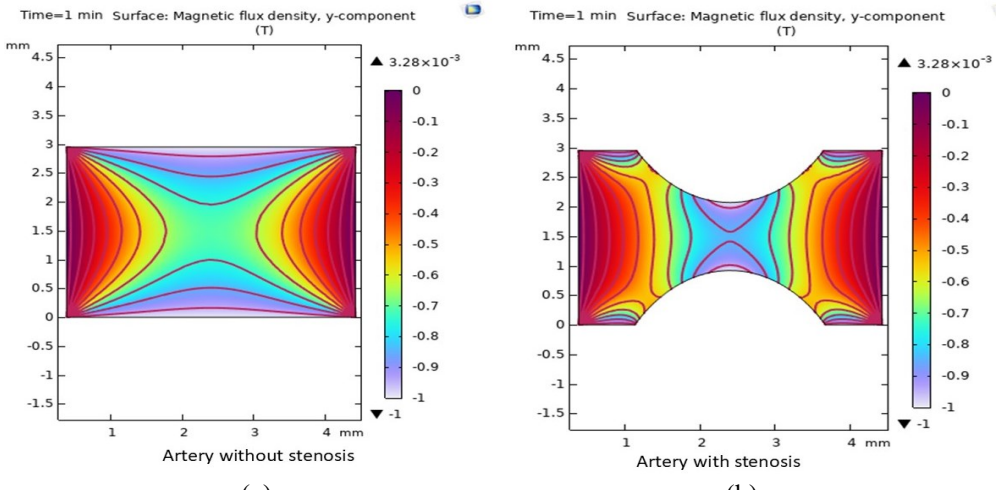

(a) (b)

Fig. 6. Distribution of magnetic field in artery (a) without stenosis, and (b) with stenosis at 1 min

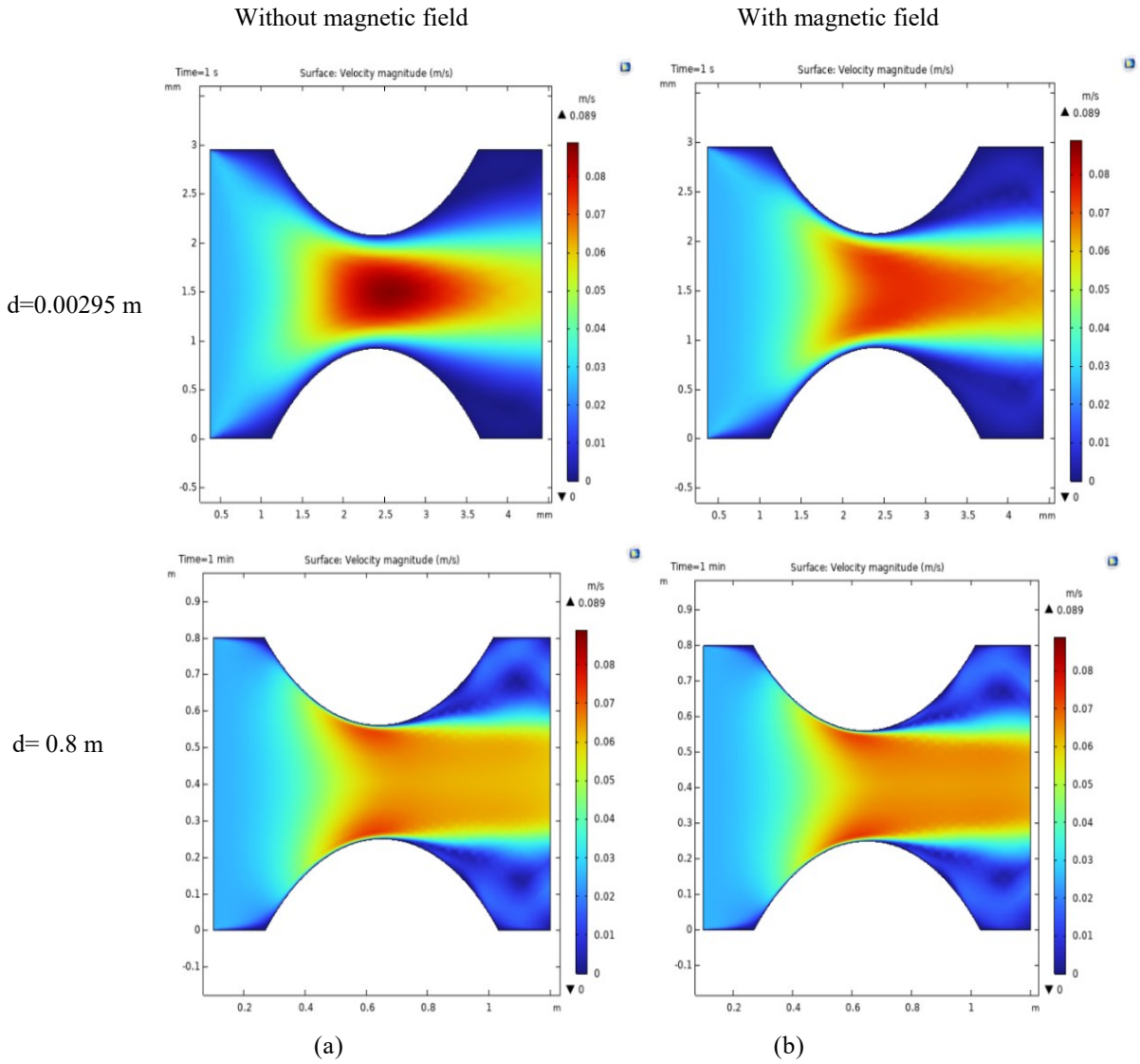

Fig. 7. Velocity of blood (a)without, and (b) with a magnetic field at 1 min.

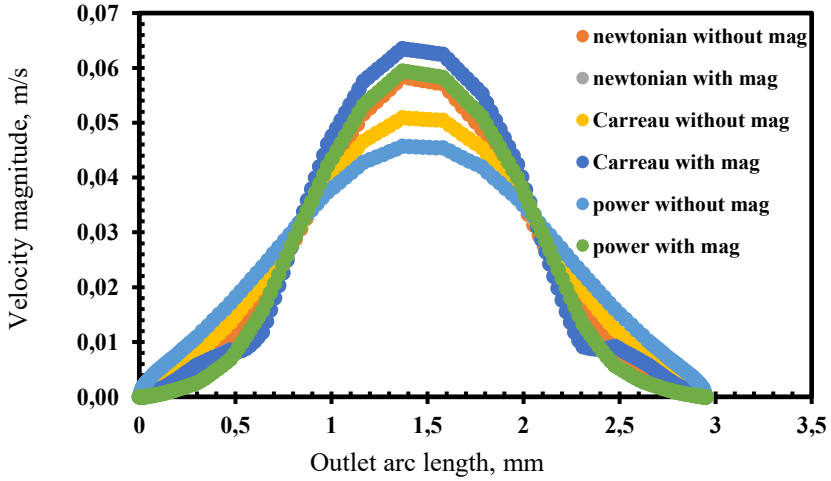

Fig. 8. Velocity profile of blood without and with a magnetic field, for different viscous models

To demonstrate the presence of stenoses and the impact of the magnetic field on the fluid domain, only the fluid domain is displayed. It has been reported that under various fluid flow conditions, the distribution of the magnetic lines changes significantly depending on the geometry's shape and the fluid's characteristics [24]. The effect of the blockage's dimensions and form on the distribution

of magnetic field lines along the geometry was observed in the present study. It was found that the simulated geometry's decreased cross-sectional area increased the magnetic field's non-uniformity. The magnetic lines got denser in the stenosis zone and near the wall. The wall has the strongest magnetic field, which weakens with distance. As a result, the field is inherently strongest close to the source of the magnetic field, i.e., nearby artery wall. The magnetic field lines converged, close to a constriction. So, a denser magnetic field was produced by this increased concentration of field lines in a restricted area.

Fig. 7 displays the blood velocity for arteries with dimensions d=0.00295 m and d=0.8 m at 1 min with and without a magnetic field using the Newtonian model. The figure clearly shows that the effect of a magnetic field with 1 Tesla on velocity was more significant for the artery with a smaller width. The dark red color depicting the maximum blood velocity without a magnetic field at the stenotic region of the artery was absent when a magnetic field was used. This showed that the maximum velocity was reduced when a magnetic field was applied. It has been cited that due to haemoglobin, which contains iron oxide, and the fact that blood is a suspension of red blood cells, it possesses magnetohydrodynamic flow properties and is electrically conductive [34]. In the presence of a magnetic field, a Lorentz force is produced, which opposes the blood motion and so decreases the blood velocity. Fig. 8 shows the comparison of velocity magnitudes along the stenotic width using different viscous models with and without a magnetic field. It can be observed that the velocity was flatter using the Power law model, as the maximum velocity was lower compared to the Newtonian model and Carreau model in the absence of a magnetic field. In the presence of a magnetic field, the maximum velocity decreased for all three models. The velocity magnitude computed with the Carreau model was similar to that of the Power law model in the presence of a magnetic field. However, it was found that the values of the Carreau model were comparable to those of the Newtonian model in the absence of a magnetic field.

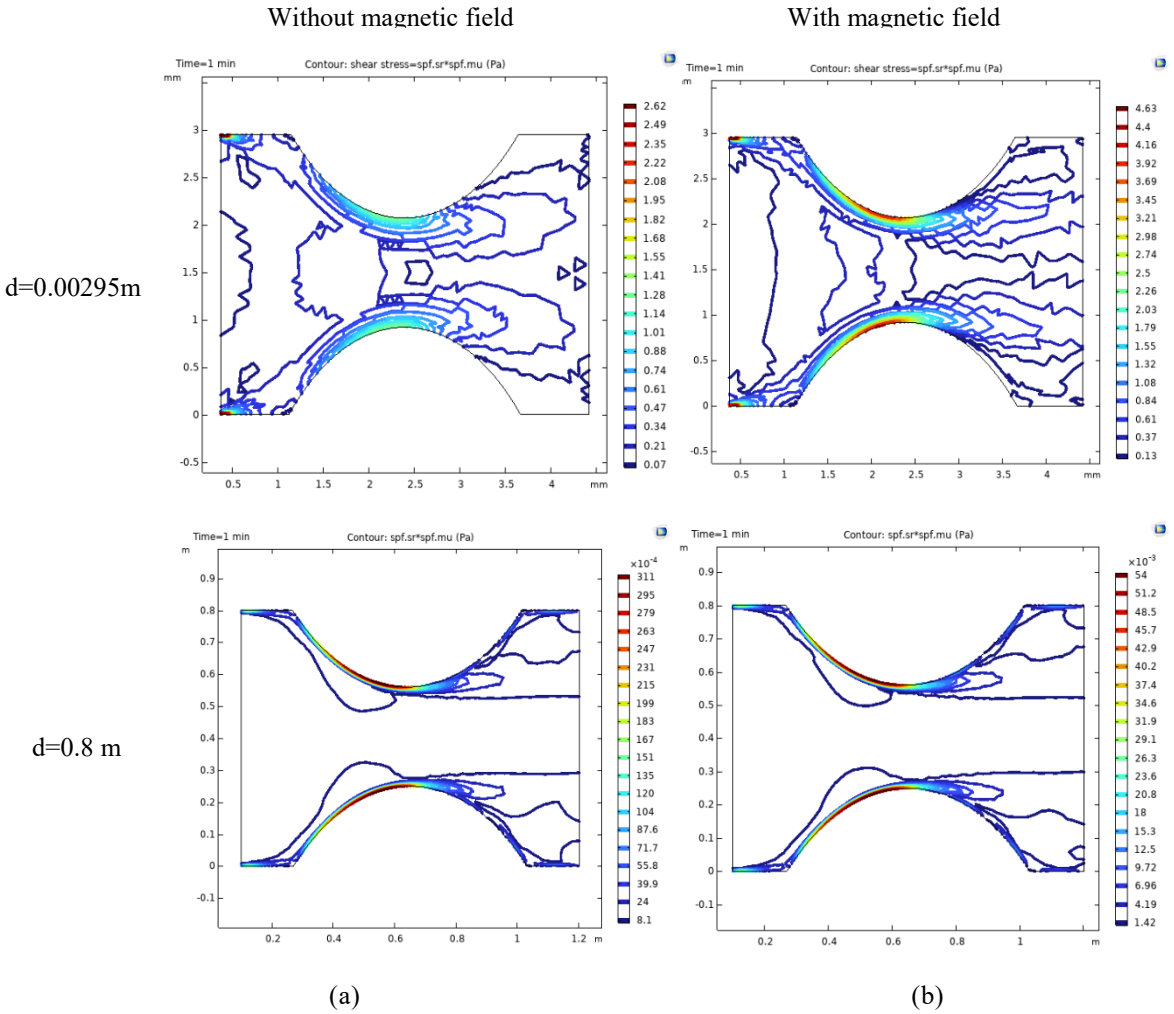

Fig 9. Shear stress of blood (a) without, and (b) with a magnetic field at 1 min

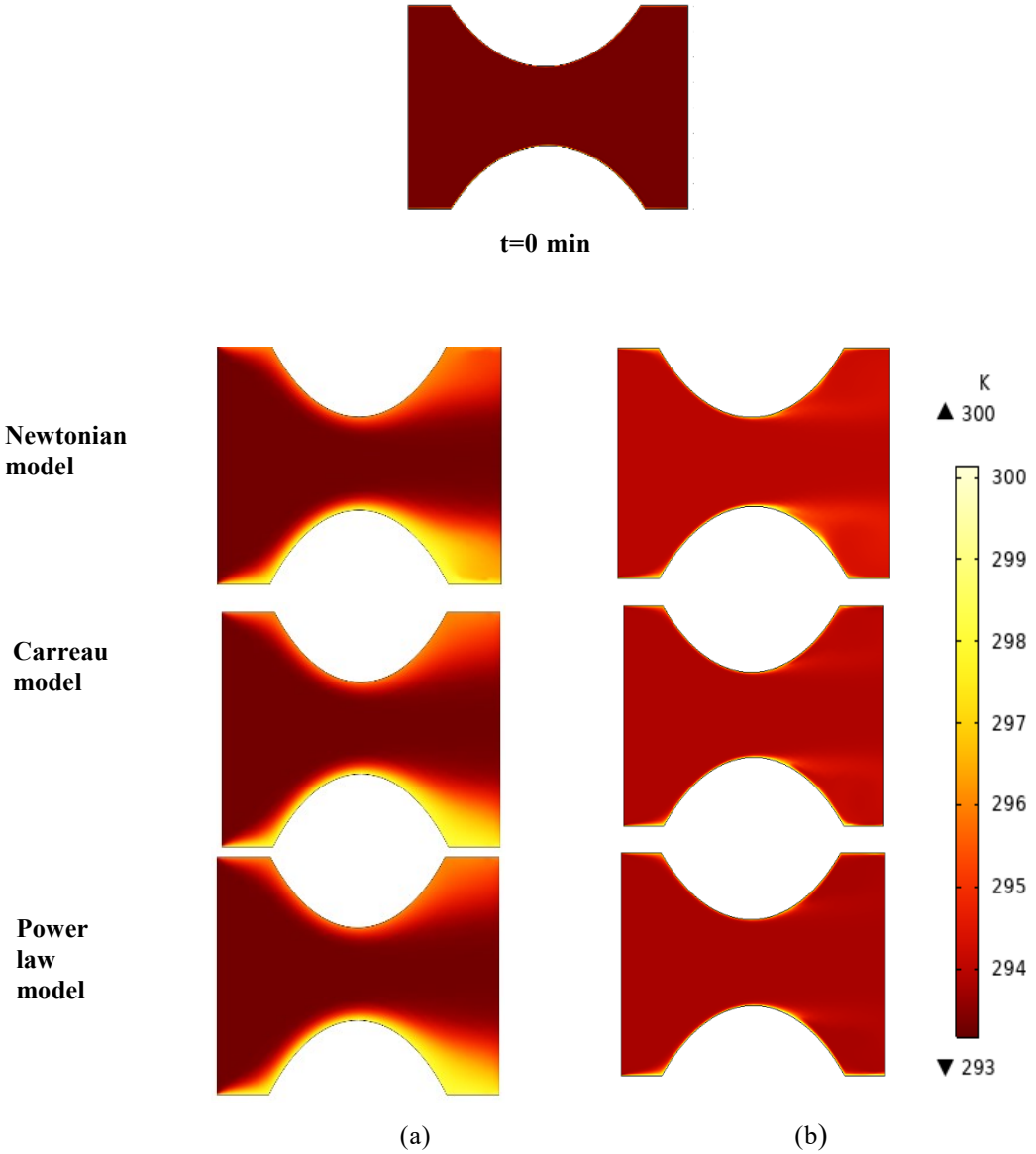

Fig. 10. Temperature in a stenotic artery in (a) d=0.00295 m, (b) d=0.8 m for v=0.025 m/s, t=1 min

Fig. 9 shows the shear stress at different arteries with and without a magnetic field. The figure demonstrates that the shear stress near the wall increases with a decrease in dimension. This is due to an increase in the viscous sublayer region in the artery, which was also observed in the velocity distribution in Fig. 5. The highest shear stress was found in the artery with d=0.00295 m under a magnetic field in the stenotic region. It has been cited in literature that, parallel to the vorticity of the flow, a magnetic moment usually has little effect on viscosity [35]. However, if the direction of vorticity is perpendicular to the magnetic field, the fixed magnetic moment in the blood can hinder free rotation. The resultant local gradients in the magnetic fluid's velocity raise the magnetic fluid's viscosity [34].

Temperature contours

The artery's radius influences blood flow and changes the rate at which heat is transferred. The effects of surgically enlarging a blocked blood vessel pose a risk to the health of the human body due to changes in blood temperature [35]. Analyzing thermal profiles can reveal problems with blood flow and tissue damage, and changes in the artery's temperature and heat transfer properties can show the course of the disease [25]. Therefore, the temperature distribution for the blood flow with nanoparticles was studied and shown in Fig. 10 for arteries with a width of 0.8 m and 0.00295 m, respectively. At time t=0, blood was at 293.15 K, and the top and bottom boundary walls were at temperatures 297.15 K and 300.15 K, respectively. Fig. 10 shows that the color of the blood temperature changed from dark red to a

lighter shade, which indicates that the temperature increased from 293.15 K to a higher value at time t=1 min. The distribution of the blood temperature changed with time because of convective heat transfer caused by blood movement and heat conduction from the walls with higher temperatures. For the case of a 0.8 m wide artery, the temperature was found to be higher (yellow color) in the region where the velocity gradient was high at 1 min. However, in the case of an artery with a width of 0.00295 m, the blood near the region of the wall was at a higher temperature (yellow color). In this case, heat transfer was mainly due to heat conduction at the viscous sublayer, where the velocity was low compared to the central region. This shows that the fluid's convective heat transfer may not be the dominant factor for heat transfer in smaller arteries.

CONCLUSIONS

Hydrodynamics and heat transfer of blood flow with silver nanoparticles in a stenotic artery were investigated. The model's findings were in accordance with the existing literature. This study demonstrated the potential significance of the viscous model for smaller arteries. The Carreau fluid exhibited Newtonian behavior at low shear rates and Power law behavior at high shear rates. When a magnetic field was introduced, the maximum velocity decreased, and the shear stress close to the wall increased, particularly for smaller arteries. Heat conduction in the viscous sublayer, where the velocity was lower than in the core region, could be the primary cause of heat transmission in smaller arteries. This model can be used for future studies such as evaluating the long-term effects of hybrid nanofluids on blood flow and heat transfer in stenotic arteries, investigating alternate nanoparticle compositions, and optimizing nanoparticle concentrations. Further research work can be conducted, considering the functionalization of silver nanoparticles with superparamagnetic elements like iron oxides, which can be made responsive to magnetic fields. This would be particularly beneficial in applications such as drug administration, stem cell distribution, and hyperthermia, where it can deliver a therapeutic substance to a target site in the human body, thereby minimizing adverse effects and enhancing therapeutic efficacy.

Acknowledgement: *With the financial support of the FRGS grant (F.35(1)(1)/2025/RDC/2975/24), the writers would like to thank Guru Gobind Singh Indraprastha University, New Delhi, for providing the necessary administrative and financial support to complete this research project.*

REFERENCES

1. N. K. Kodali, L. D. Bhat, N. E. Phillip, S. F. Koya, *Indian Heart J*., **75**(1), 31 (2023).
2. T. Hayat, S. Nadeem, *Results Phys*., **7**, 2317 (2017).
3. H. Waqas, U. Farooq, A. Hassan, D. Liu, S. Noreen, R. Makki, M. Imran, M.R. Ali, *Results Phys*., **44**, 106152 (2023).
4. S. Nadeem, S. Ijaz, *AIP Adv.,* **5**, 107217 (2015).
5. S. Nadeem, S. Ijaz, M. A. Sadiq, *Curr. Nanosci*., **10**(5), 753 (2014).
6. A.F. Elelamy, N.S. Elgazery, R. Ellahi, *Int. J. Numer. Methods Heat Fluid Flow*, **30**(11), 4883 (2020).
7. A. Hussain, L. Sarwar, A. Rehman, S. Akbar, F. Gamaoun, H.H. Coban, A.H. Almaliki, M.S. Alqurashi, *Appl. Sci.,* **12**(3), 1601 (2022).
8. R. Kotcherlakota, S. Das, C. R. Patra, in: Green Synthesis, Characterization and Applications of Nanoparticles, A. K. Shukla, S. Iravani (eds.) Elsevier, 2019.
9. Y. Haik, C. J. Chen, J. Chatterjee, *J. Vis*., **5** (2), 187 (2002).
10. K. Teimouri, M. R. Tavakoli, A. Ghafari, K. C. Kim, *Comput. Biol. Med.*, **135**, 104600 (2021).
11. L. Pauling, C. D. Coryell, *Proc. Natl. Acad. Sci.* **22** (4), 210 (1936).
12. V. Zablotskii, T. Polyakova, A. Dejneka, *Cells*, **11** (1), 81 (2022).
13. Y. Haik, V. Pai, C.J. Chen, *J. Magn. Magn. Mater.*, **194** (1), 254 (1999).
14. Xenos, M. A., E. E. Tzirtzilakis, *Adv. Dyn. Syst. Appl.* **8**(2), 427 (2013).
15. B. Tashtoush, A. Magableh, *Heat Mass Transf.,* **44** (3), 297 (2008).
16. G. Varshney, V. Katiyar, S. Kumar, *Int. J. Eng. Sci. Technol.* **2**(2), 967 (2010).
17. M.G. Reddy, O.D. Makinde, *J. Mol. Liq*., **223**, 1242 (2016).
18. A. Meher, A. Tandi, S. Moharana, S. Chakroborty, S. S. Mohapatra, A. Mondal, S. Dey, P. Chandra, *Hybrid Advs*., **6**, 100184 (2024).
19. A. A. H. El-Bassuony, H. K. Abdelsalam, *Phys. Scr.,* **98** (5), 055919 (2023).
20. S. W. I. Onwuzu, A. C. Ugwu, G. C. E. Mbah, I. S. Elo, *Radiography,* **27** (2), 581 (2021).
21. S. S. Ghadikolaei, M. Yassari, H. Sadeghi, Kh. Hosseinzadeh, D. D. Ganji, *Powder Technol*., **322**, 428 (2017).
22. S. S. Ghadikolaei, M. Gholinia, M. E. Hoseini, D. D. Ganji, *J. Taiwan Inst. Chem. Engrs*., **97**, 12 (2019).
23. E. P. Furlani, Permanent Magnet and Electromechanical Devices: Materials, Analysis, and Applications, Academic Press, 2001.
24. C. S. Maurya, A. Kumar, *Comput. Biol. Med*., **184**, 109464 (2025).
25. S. Pabi, Mohd. K. Khan, A. Raj, *Int. Commun. Heat Mass Transf.*, **159**, 108236 (2024).

26. B. M. Johnston, P. R. Johnston, S. Corney, D. Kilpatrick, *J. Biomech*., **37** (5), 709 (2004).
27. M. Siebert, P. Fodor, *Proceedings of the COMSOL Conference, Boston*, **27** (2009).
28. S. Lynch, N. Nama, C. A. Figueroa, *Sci. Rep*., **12** (1), 20568 (2022).
29. J. Xiang, M. Tremmel, J. Kolega, E. I. Levy, S. K. Natarajan, H. Meng, *J. Neurointerv. Surg.*, **4** (5), 351 (2012).
30. N. O. Ajayi, L. Lazarus, E. A. Vanker, K. S. Satyapal, *Int. J. Morphol*., **31** (4), 1393 (2013).
31. J. T. Dodge, B. G. Brown, E. L. Bolson, H. T. Dodge, *Circulation,* **86** (1), 232 (1992).
32. B. M. Johnston, P. R. Johnston, S. Corney, D. Kilpatrick, *J. Biomechanics,* **39** (6), 1116 (2006).
33. M. R. Sadeghi, M. Jahangiri, M. Saghafian, *J. Braz. Soc. Mech. Sci. Eng.*, **42** (11), 570 (2020).
34. S. Sharma, U. Singh, V. K. Katiyar, *J. Magn. Magn. Mater*., **377**, 395 (2015).
35. X. Liu, X. Chen, Y. Zhang, J. Xie, X. Jia, T. Deng, Y. Zheng, T. Davood, Z. Majid, *Alex. Eng. J*., **61** (9), 7195 (2022).